Effect of polymeric matrix in anion-exchange membranes on nitrate-chloride separations

Separation and Purification Technology

Chinello, Daniele; Post, Jan; de Smet, Louis C.P.M.

https://doi.org/10.1016/j.seppur.2024.129440

Separation and Purification Technology 355 (2025) 129440

Contents lists available at ScienceDirect

Separation and Purification Technology

journal homepage: www.elsevier.com/locate/seppur

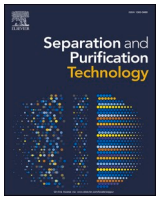

Effect of polymeric matrix in anion-exchange membranes on nitrate-chloride separations

Daniele Chinello [a,b], Jan Post [a], Louis C.P.M. de Smet [a,b,*]

[a] Wetsus, European Centre of Excellence for Sustainable Water Technology, Oostergoweg 9, Leeuwarden 8911 MA, the Netherlands
[b] Advanced Interfaces & Materials, Laboratory of Organic Chemistry, Wageningen University, Stippeneng 4, Wageningen 6708 WE, the Netherlands

ARTICLE INFO

Editor: Dr. B. Van der Bruggen

Keywords:
Ion-exchange membranes
Nitrate/chloride selective separation
Dehydration energy
Electrodialysis

ABSTRACT

Selective separation of monovalent ions such as nitrate from chloride using Anion-Exchange Membranes (AEMs) is challenging. Previously, we showed that an increased polyvinylidene fluoride (PVDF) concentration in AEMs manufactured with an anion-exchange ionomer solution (Fumion FAS-24) increased nitrate over chloride selectivity. The membrane containing 50 wt% of PVDF showed higher selectivity compared to two commercial membranes (AMX and ACS from Neosepta) when tested in electrodialysis. This improved selectivity was associated with increased hydrophobicity of the membrane, facilitating the permeation of less hydrated ions such as nitrate.

However, due to concerns regarding per- and polyfluoroalkyl substances (PFAS), there is a quest for substitutes for fluoropolymers. In this study, we investigated whether using alternative polymers to PVDF influences nitrate/chloride separation performance. Polyvinyl chloride (PVC) and polyacrylonitrile (PAN) were blended with Fumion FAS-24 to manufacture new AEMs. The nitrate/chloride selective separation performance of these membranes was tested in electrodialysis and compared with the recently introduced PVDF-based AEM.

Results show that although the PVDF-based membrane presents higher hydrophobicity, the PAN-based membrane possesses slightly lower selectivity, while the PVC-based membrane exhibits higher nitrate selectivity. This study proves that increasing the membrane hydrophobicity is a valid strategy to increase selectivity toward nitrate. However, it also suggests that other parameters, such as fixed charge concentration, can play a role. Therefore, balancing properties such as hydrophobicity and fixed charge concentration is imperative to achieving optimal selectivity and performance when developing ion-selective membranes.

1. Introduction

Ion-exchange membranes (IEMs) have considerable importance in membrane-based technology such as electrodialysis (ED) [1–3], capacitive deionization [4–6], and fuel cells [7,8]. These membranes are made from polymer materials and contain charged moieties. Depending on the type of charge of these groups, IEMs can be categorized into two main types: Anion-Exchange Membranes (AEMs) and Cation-Exchange Membranes (CEMs). AEMs feature fixed cations such as quaternary ammonium groups, and allow the permeance of anions while impeding cations. In contrast, CEMs possess anionic moieties like sulfonic groups, allowing the permeation of cations while hindering anions.

IEMs find extensive use in various separation technologies, such as desalination [9–11], and in this study we focus on AEMs for the application of electrodialysis (ED). AEMs have already proved to be effective in the separation of monovalent from divalent ions [12]. However, the separation of two monovalent ions poses a larger challenge, especially if these ions present similar hydrated radius and hydration energy, such as nitrate and chloride (Table 1). Developing membranes possessing high monovalent/monovalent selectivity is crucial in applications such as the recovery and recycling of important resources like nitrate from, e.g., waste/process water streams in fertilizer plants [13] and horticulture [14], with the overarching aim of achieving a circular economy.

In order to increase the membrane's ability to discriminate between ions bearing the same valence, previous studies [15–18] focused on leveraging the difference in the ion dehydration. Ions with lower dehydration energy, such as nitrate (Table 1), are more favourable

* Corresponding author at: Advanced Interfaces & Materials, Laboratory of Organic Chemistry, Wageningen University, Stippeneng 4, Wageningen 6708 WE, the Netherlands.
E-mail address: louis.desmet@wur.nl (L.C.P.M. de Smet).

https://doi.org/10.1016/j.seppur.2024.129440
Received 8 May 2024; Received in revised form 28 August 2024; Accepted 29 August 2024
Available online 5 September 2024

Table 1
Ionic radii, hydrated radii and hydration energies of nitrate, and chloride [69].

Anion	Ionic radius [nm]	Hydrated radius [nm]	Hydration energy [kcal·mol^{-1}]
Nitrate (NO_3^-)	0.264	0.335	71
Chloride (Cl^-)	0.181	0.332	81

transported through the AEMs due to an easier (partial) dehydration at the membrane surface [19–22]. In particular, these mostly e-driven separation studies indicate that an increased membrane hydrophobicity triggers the dehydration of ions with lower dehydration energy, while more hydrated ions are hindered by the hydrophobic structure.

Furthermore, the strength of the interaction between the dehydrated ion and the charged groups within the membrane is a determining factor in the dehydration process. A stronger interaction has been observed to reduce the associated energy barrier, since it leads to an energetically more favorable state of the ion [23,24]. However, this electrostatic interaction also influences the ion's mobility. Specifically, the stronger the interaction, the slower the transportation [23,24].

Building further on these findings, we studied, in previous research [25], the transport of nitrate and chloride using newly developed PVDF-based AEMs, manufactured in combination with an anion-exchange ionomer solution (Fumion FAS-24, FUMATECH BWT GmbH). PVDF was chosen for its intrinsic hydrophobic nature and its wide application in membrane technology such as membrane distillation [26–32], dye removal from water streams using nanofiltration [33–35], oil–water separation [36,37], organic pollutant removal [38,39], selective ion separation [40–46], and removal of toxic metal ions from aqueous streams [47,48]. PVDF has also been used in selective ion-separation applications, such as fabricating electrodes for capacitive deionization (CDI) to separate divalent from monovalent cations [40–42]. Additionally, it has also been used in manufacturing AEMs for example in combination with cross-linked quaternized polyepichlorohydrin for selective hydroxide ion transport in fuel cells [49], and with styrene-co-vinylbenzyl chloride for water desalination in ED [50]. Furthermore, PVDF has been combined with morpholine-functionalized vinyl benzyl chloride for acid recovery by diffusion dialysis [51] and with polyaniline for desalination in ED and CDI. However, the use of PVDF for manufacturing membranes specifically designed for the selective separation of monovalent ions like nitrate and chloride has not been documented in the literature, except in our previous studies [52,53].

In those studies, our focus was on investigating the influence of different PVDF content levels in the membranes, ranging from 0 to 50 wt %. The outcomes of that work revealed an improved nitrate affinity with increasing PVDF concentration, and thus membrane hydrophobicity, with the membrane containing 50 wt% PVDF reporting the highest nitrate permeability. However, by increasing the PVDF content, we also noted an increase in the membrane's electrical resistance, and for this reason, we decided not to exceed 50 wt% of PVDF. The performance of this membrane was then investigated in ED [53]. Experimental data showed higher values of the nitrate over chloride selectivity compared with two commercial membranes (AMX and ACS from Neosepta), the highest reported in literature.

However, considering that Per- and polyFluoroAlkyl Substances (PFAS) pose a significant environmental and health concern due to their persistent nature and widespread contamination [54–56], alternatives for fluoropolymers become imperative to mitigate the adverse effects of PFAS exposure, safeguard human health [57,58], and reduce the long-term environmental impact associated with these persistent chemicals.

For this reason, we decided to now investigate the impact of the type of the polymer used in combination with the ionomer solution Fumion FAS-24 to manufacture new AEMs. Specifically, we opted for polyvinyl chloride (PVC) and polyacrylonitrile (PAN) as alternatives to PVDF. PVC was selected for its presence in commercial membranes as reinforcement material, solubility in N-methyl-2-pyrrolidone (NMP), the solvent of the ionomer solution, and cost-effectiveness [59,60], making it an attractive alternative for large-scale applications where cost efficiency is crucial. PVC has already been used in the manufacturing of membranes [61], including AEMs [62]. For example, Nemati *et al.*[63] modified the properties of PVC-AEMs by incorporating TiO_2 nanoparticles (0–4 wt%) to improve the anion permeation efficiency and tested them in ED. The study reported improved permeation of chloride and sulfate in the TiO_2 concentration interval of 0.5–2 wt%. Liu *et al.* [64] used PVC to manufacture films by casting, which were then modified by immersing these films in a solution of triethylenetetramine, obtaining AEMs. These AEMs showed good stability and antifouling potential. Moreover, when applied in ED, the optimized PVC-AEM demonstrated a NaCl removal ratio of 90 %, outperforming a commercial membrane (JAM-II-5 AEM). Recently, Zafari *et al.* [65] prepared heterogeneous AEMs by combining PVC and an anion-exchange resin (Amberlite IRA-410). The surface of these membranes was subsequently modified through a three-step process, including plasma treatment and coupling with polyethylenimine and glutaraldehyde. By changing the surface hydrophilicity of the membranes, they increased the membrane selectivity towards formate ($CHOO^-$) over oxalate ($C_2O_4^{2-}$) — exploiting the lower hydration energy of the former — reaching a selectivity value of 4.3 in ED.

PAN was also chosen for its solubility in NMP, and for its potential for further modification of the nitrile groups [66–68]. The characteristics of these new membranes together with the nitrate/chloride separation performance in ED are evaluated in this study and compared with the previously introduced PVDF membrane.

2. Materials and methods

2.1. Chemicals

Polyvinyl chloride (average $M_w \sim 233{,}000$ by GPC, powder form) (PVC), polyacrylonitrile (PAN) (average $M_w \sim 150{,}000$ by GPC, powder form), sodium chloride (ACS reagent, ≥99.0 %), sodium nitrate (ACS reagent, ≥99.0 %), sodium sulphate (ACS reagent, ≥99.0 %, anhydrous), were purchased from Sigma Aldrich and used as received. N-methyl-2-pyrrolidone (NMP, HPLC grade 99.5 %) was purchased from Alfa Aesar. Fumion FAS (24 wt% solution in NMP), which physicochemical properties are reported in **Table S1** of the Supporting Information, was purchased from FUMATECH BWT GmbH, Bietigheim-Bissingen, Germany. The Neosepta AMX, ACS and CMX membranes were purchased from ASTOM Corporation, Tokyo, Japan. The physicochemical properties of these commercial membranes are reported in **Table S2** of the Supporting Information.

2.2. Membrane fabrication

The AEMs were manufactured following the procedure reported in our previous study [25]. Each membrane is composed of 50 wt% of ionomer (Fumion FAS-24) and 50 wt% of the selected polymer (PVC or PAN). This ratio was selected in order to enable direct comparison with the PVDF-based membrane composed of 50 wt% of ionomer and 50 wt% of PVDF, labelled as PVDF-50, investigated in our previous studies [52,53]. Specifically, 0.75 g of ionomer were mixed with 0.75 g of PVC or PAN. NMP was used as solvent to dissolve the polymers, obtaining solutions with a concentration of 16 wt%. The solvent was removed by casting the solutions onto a glass plate kept at 60 °C for 24 h. To completely remove the solvent, the obtained membranes were immersed in 0.5 M NaCl, refreshing the solution every 2 h (5 ×). During this phase, the thickness of the wet membranes was measured using a digital thickness gauge (Mitutoyo Corporation, model no. ID-C112BS). The membranes were stored in 0.5 M NaCl and labelled as PVC-50 and PAN-50, where the number indicates the weight percentage of polymer, PVC

or PAN, present in the membrane. Selected characteristics, together with those of the previously introduced PVDF membrane, labelled PVDF-50, are reported in Table 2.

3. Membrane characterization

3.1. Water uptake (WU)

To assess water uptake (*WU*), we followed the methodology outlined in our previous work [25]. After immersing the membrane in demineralized water for 24 h, the mass of the wet membrane was recorded after removing any surface water with a tissue. Subsequently, the membrane was dried in an oven maintained at 55 °C for 24 h. The mass of the resulting dry membrane (W_{dry}, in grams) was then recorded. The water uptake (*WU*) was calculated as a percentage by:

$$WU = 100 \times \frac{W_{wet} - W_{dry}}{W_{dry}}\% \quad (1)$$

3.1.1. Ion-exchange capacity (IEC)

The quantity of fixed charged groups within an AEMs can be determined indirectly by measuring the concentration of counterions exchanged with a specific solution. In particular, following a 48 h conditioning period in 0.5 M NaCl, the selected membrane was immersed in the exchange solution (200 mL of 0.5 M $NaNO_3$) after a rapid immersion in demineralized water to eliminate the excess of NaCl solution. After a 24-hour exchange duration, the chloride concentration in the solution was assessed through ion chromatography (IC), using a Metrohm Compact IC 761 equipped with a conductivity detector and chemical suppression.

The ion-exchange capacity (*IEC*) of the membrane, expressed in milliequivalents per gram ($meq \cdot g^{-1}$), was then calculated according to the following equation [70]:

$$IEC = \frac{n_{eq}}{W_{dry}} \quad (2)$$

where n_{eq} denotes the equivalent of exchanged ions in equivalents (eq), and W_{dry} (g) represents the dry mass of the membrane.

3.2. Fixed charge concentration (FCC)

By using the values of the *IEC* and *WU*, it is possible to calculate the fixed charge concentration (*FCC*) of the hydrated membranes, which refers to the density of charged groups expressed in terms of moles per volume of adsorbed water ($mol \cdot L^{-1}$). The *FCC* was calculated according to the following equation [71]:

$$FCC = \frac{IEC}{WU/100} \times \rho_w \quad (3)$$

where ρ_w is the density of the water in the membrane, typically assumed to be equivalent to the density of pure water.

3.3. Electrical resistance

The electrical resistance of the manufactured IEMs was evaluated according to the protocol established by Galama *et al.* [72], by using a six-compartment cell as schematically outlined in **Figure S1** in the Supporting Information. The membrane configuration in the setup consists of four CEMs, specifically CMX from Neosepta, while the AEM under investigation separates compartments A and B. An electrolyte solution such as 0.5 M NaCl was recirculated in compartments A, B, and C at 170 $mL \cdot min^{-1}$, while in compartment D, 0.5 M Na_2SO_4 was used. A potentiostat (Autolab AUT72398, Metrohm) with a four-electrode configuration was used to apply a current between the two Pt/Ir electrodes situated in compartments D. The potential across the membrane was recorded by using two Haber–Luggin capillaries (outer diameter 4.0 mm, inner diameter 2.0 mm) placed on the side of the membrane under investigation and connected to Ag/AgCl electrodes.

Specifically, the current (*I*) is increased gradually from 1 to 25 mA. For each value, the current is applied for 2 min to equilibrate the system, with the potential (*V*) recorded during the final 8 s. Iterating this process across all current values results in a potential/current graph. The angular coefficient of the extrapolated equation obtained from the data interpolation in the graph represents the electrical resistance (*R*) of the membrane (Ω) according to Ohm's law:

$$V = R \times I \quad (4)$$

However, this value also includes the electrical resistance generated by the 0.5 M NaCl electrolyte solution. Therefore, by removing the membrane under investigation between compartments A and B, it is possible to determine this contribution (R_s), which is then subtracted from the one obtained in the experiment involving the membrane. This process yields the specific electrical resistance of the membrane (R_m):

$$R_m = R - R_s \quad (5)$$

This value was then multiplied for the membrane's active area to obtain the membrane area resistance ($\Omega \cdot cm^2$).

3.4. Contact angle

In order to evaluate the surface hydrophobicity, contact angles were

Table 2
Chemical and physical properties of the PVC-50 and PAN-50 membranes investigated in this study, along with those of PVDF-50 [53].

Membrane	Composition (wt%:wt%)	Polymer Structure	Thickness (μm)	*IEC* ($meq \cdot g^{-1}$)	*WU* (%)	*FCC* ($mol \cdot L^{-1}$)	Electrical Resistance ($\Omega\ cm^2$)
PAN-50	PAN:Fumion FAS-24 = 50:50	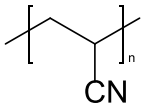	100–105	0.75 ± 0.01	15.0 ± 0.4	5.0 ± 0.2	8.8 ± 0.1
PVC-50	PVC:Fumion FAS-24 = 50:50	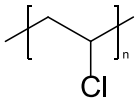	95–100	0.72 ± 0.01	9.5 ± 0.4	7.7 ± 0.3	9.4 ± 0.1
PVDF-50	PVDF:Fumion FAS-24 = 50:50	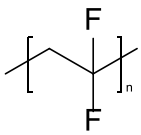	80–85	0.74 ± 0.02	6.5 ± 0.8	11.0 ± 0.8	11.5 ± 0.3

measured through the captive bubble method. In this method, an air bubble (1 μL) is introduced beneath the membrane surface immersed in water, using a needle with a hook-like shape. The contact angles were then determined by analyzing the shape of the bubble at the membrane surface interface, using a contour analysis system (OCA35, DataPhysics Instruments, Germany). For each membrane, six drops at different locations were analyzed.

3.5. SEM-EDX

The surface morphology of the three membranes was examined through scanning electron microscopy (SEM) employing a JEOL JSM-6480LV electron microscope at 10 kV acceleration. Additionally, to evaluate the polymer distribution within the membranes, the elemental distribution of fluorine, chlorine, and nitrogen, was examined respectively for the PVDF-50, PVC-50, and PAN-50 membranes using an energy-dispersive X-ray spectrometer (EDX).

3.6. Membrane performance

3.6.1. Permselectivity

The permselectivity refers to the ability of a membrane to selectively allow counterions while hindering co-ions. Following the procedure of Duglokecki *et al.* [70], the permselectivity of the manufacture AEMs was assessed in a two-compartment cell made of poly(methyl 2-methylpropenoate) (PMMA), with a total solution volume of 0.2 L. Specifically, the potential across the membrane separating two electrolyte solutions (0.1 M and 0.5 M NaCl, respectively) recirculating at a flow rate of 750 $mL{\cdot}min^{-1}$ was recorded using Ag/AgCl electrodes immersed in the solution. Subsequently, the membrane permselectivity (α), expressed as a percentage, was calculated using the following equation:

$$a = 100 \times \frac{\Delta V_{measured}}{\Delta V_{theoretical}} \tag{6}$$

where $\Delta V_{theoretical}$ is the theoretical Nernst membrane potential for a membrane 100 % selective towards counterions.

3.6.2. Permeability coefficients ratio

The permeability coefficients ratio serves as a measure of the affinity between a membrane and two distinct counterions, providing a quick indication of the membrane selectivity. The experimental setup employed to determine this parameter mirrors that used for the permselectivity experiments. However, while on one side of the membrane a 0.1 M NaCl solution is still used, on the other side a 0.1 M $NaNO_3$ solution is present now. The potential across the membrane was continuously monitored for a duration of 40 min using a Ag/AgCl electrodes. For the calculation, the averaged potential ($\Delta\Psi$) obtained after reaching steady-state conditions, approximately 10 min into the experiment, was utilized. The permeability coefficient ratio was determined using the following equation [25,73]:

$$\frac{P_{NO_3^-}}{P_{Cl^-}} = e^{\frac{F\Delta\Psi}{RT}} \tag{7}$$

where F is the Faraday constant (96,458 $A{\cdot}s{\cdot}mol^{-1}$), R is the universal gas constant (8.314 $J{\cdot}mol^{-1}{\cdot}K^{-1}$), T is the absolute temperature (K), and $P_{NO_3^-}$ and P_{Cl^-} are the permeability coefficients of the counterions.

3.6.3. Electrodialysis experiments

In order to assess the performance of the manufactured AEMs in electrodialysis (ED) and thus determine the nitrate over chloride selectivity, the experimental setup and procedure reported in our previous work were used [53]. The membrane configuration of the ED setup is reported in Fig. 1, and consists of a total of five IEMs; three cation-exchange membranes (CMX from Neosepta) are alternated with two of the manufactured AEMs (PVC-50, or PAN-50), resulting in two cell pairs.

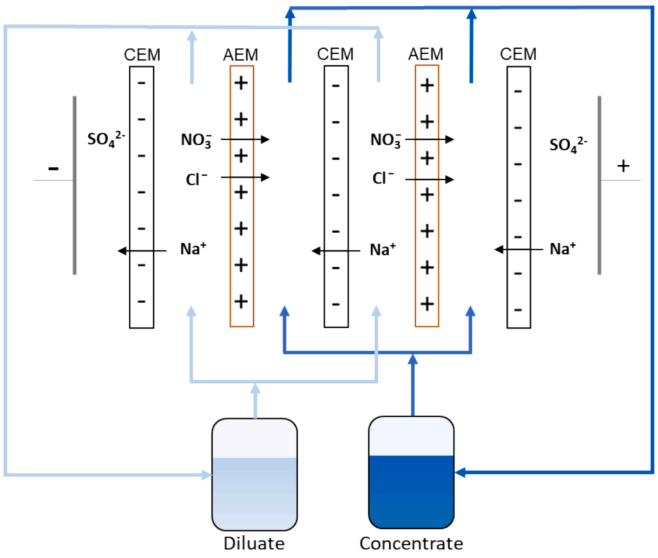

Fig. 1. Schematic representation of the ED setup used to determine the nitrate over chloride selectivity of the manufactured PVC-50 and PAN-50 AEMs. See **Section 2.9.3** for a detailed explanation of the system. Light and dark blue stand for diluate and concentrate stream, respectively.

Each membrane is separated from the adjacent one by a gasket with an integrated spacer, which has a thickness of 0.5 mm, and the available membrane area for ion transport is 20 cm^2.

Two platinum-coated titanium mesh electrodes are present in the setup, with a solution of 1 L of 0.1 M Na_2SO_4 recirculating in these compartments. In the outlets of the electrode compartments, two Ag/AgCl electrodes are placed to measure the potential across the five membranes.

The experiments are carried out in batch mode with a current density set at 20 $A{\cdot}m^{-2}$, employing a potentiostat (Autolab AUT72157, Metrohm) as the current source. Experiments were conducted in triplicate for each membrane, with a duration of 3 h, corresponding to a theoretical anion removal of 90 %. The initial composition of the electrolyte solutions in the two reservoirs is 0.1 L of 0.05 M $NaNO_3$ and 0.05 M of NaCl.

Samples from the diluate and the concentrate reservoirs were taken at intervals of 30 min and analysed by ion chromatography (IC) to determine the ion concentrations. The values obtained were used to assess the nitrate over chloride selectivity ($S_{Cl^-}^{NO_3^-}$) over time, employing the equation reported in a previous contribution in literature [16,25,53]:

$$S_{Cl^-}^{NO_3^-} = \left(\frac{\Delta C_{NO_3^-}}{\Delta C_{Cl^-}}\right)_{Concentrate} \times \left(\frac{C_{Cl^-}}{C_{NO_3^-}}\right)_{Diluate} \tag{8}$$

where $\Delta C_{NO_3^-}$ and ΔC_{Cl^-} refer to the change of the concentration of the indicated ion in the concentrate reservoir between two samples, while $C_{NO_3^-}$ and C_{Cl^-} represent the concentration of the ions in the diluate compartment. Theoretically, the concentration of nitrate and chloride in the diluate compartment to be used should ideally be the one at the membrane surface [21]. However, it is commonly accepted in literature to approximate these concentrations to the concentration in the bulk solution [74,75]. Therefore, at high degree of desalination this equation might present limitations due to the presence of the concentration polarization effect [76]. However, in order to allow a direct comparison of our results with those reported in literature, concentration polarization effects are neglected and the concentrations of the ions are approximated to those in the bulk throughout the entire ED process.

Another relevant parameter from an application point of view is the recovery ratio (R_i), which for an ion (i) is calculated according to the

equation reported by Chen *et al.*[77]:

$$R_i = \frac{V_{ct}(C_{ct} - C_{c0})}{V_{d0}C_{d0}} \times 100 \quad (9)$$

here, C_{ct}, C_{c0} and C_{d0} represent the concentrations of the ion at time t and 0, respectively, in the concentrate and dilute streams. Similarly, V_{ct} and V_{d0} denote the volumes in the concentrate and dilute at time t and 0, respectively.

The coulombic efficiency (η) of the experiments was calculated according to the equation:

$$\eta = (J_i + J_j)\frac{F}{i} \quad (10)$$

where F is the Faraday constant (96,458 A·s·mol^{-1}), i is the current density applied (A·m^{-2}), and J_i and J_j are the ionic fluxes, expressed in mol·m^{-2}·s^{-1}, across the membranes for the two counterions, which, for a monovalent ion (i), is defined by the following equation:

$$J_i = \frac{V}{A} \times \frac{\Delta C_i}{\Delta t} \quad (11)$$

where V (m^3) and ΔC_i (mol·L^{-1}) are respectively the volume and the variation of the ion concentration in the concentrate stream, A (m^2) is the surface membrane area, and Δt (s) is the time of the experiments.

Lastly, the energy consumption (E) was measured according to our previous work [53] in kilojoules per gram of nitrate recovered, using the following equation

$$E = \frac{\Delta V_{stack} \cdot i \cdot A \cdot \Delta t}{\Delta n_{NO_3^-} \cdot MW_{NO_3^-}} \quad (12)$$

where ΔV_{stack} represents the average stack potential (V), i is the applied current density (A·m^{-2}), A is the membrane surface area (m^2), Δt denotes the duration of the experiments (s), $\Delta n_{NO_3^-}$ is the change in moles of nitrate in the concentrate stream, and $MW_{NO_3^-}$ is the molecular weight of nitrate (g·mol^{-1}).

4. Results and discussion

4.1. Membrane characterization

4.1.1. Membrane preparation

Two membranes were successfully manufactured via casting by mixing the selected polymer (PVC or PAN), with the ionomer solution (Fumion FAS-24) in a ratio 50:50. This ratio was selected accordingly to our previous studies on PVDF-based membrane [25,53], in such a way to compare membranes with the same amount of ionomer, and therefore focusing on the influence of the non-charged polymer added (PVDF, PVC, or PAN). The two membranes manufactured in this study are labelled as PVC-50 and PAN-50, and Table 2 reports some of the chemical and physical properties of the PVC-50 and PAN-50 membranes investigated in this study, along with those of the PVDF-50 membranes obtained in our previous work [53].

4.1.2. IEC, WU, and FCC

As reported in Table 2, the *IEC* values for the three membranes are reasonably similar. This aligns with our expectations, considering that the same amount of ionomer solution (Fumion FAS-24) and polymers (PVC, PAN, and PVDF) were used for all membranes. Considering that the *IEC* influences the *WU* — typically membranes with high *IEC* present high values of the *WU* [78–82] — in the case of the membranes under investigation, the variation of the *WU* among the membranes can be attributed to the different nature of the polymers used. Indeed, as expected, the PVDF-50 membrane exhibits the lowest water sorption due to the inherently higher hydrophobic nature of the polymer PVDF [83–86]. Moreover, we can also observe that the water uptake trend aligns with that of the wet membrane thickness, *i.e.* PAN-50 > PVC-50 > PVDF-50, where membranes with higher water uptake present higher thickness. Additionally, combining the *IEC* and *WU* allows one to calculate the fixed charge concentration (*FCC*) of the membranes. As evident from Table 2, with the *IEC* being constant, the trend of *FCC* aligns inversely with that of *WU*, following the order PAN-50 < PVC-50 < PVDF-50. Therefore, since the distance-dependent electrostatic interaction between the mobile counterions and the fixed charged groups in the membrane follows Coulomb's law [23,87], within the PVDF-50 membrane, the counterions can experience a larger electrostatic interaction due to the higher *FCC*.

4.1.3. Electrical resistance

The membrane electrical resistance values reported in Table 2 show the following trend: PVDF-50 > PVC-50 > PAN-50. Given the similar *IEC* values for the various membranes, and considering that a correlation exists between the *IEC* and the electrical resistance [88] – membranes with higher *IEC* values exhibit lower electrical resistance – this result indicates that the electrical resistance is influenced by the nature of the polymer. In this context, it is worth comparing the manufactured membranes with two commercial membranes such as AMX and ACS from Neosepta. These commercial membranes possess *IEC* values of 2.1 and 1.9 mmol·g^{-1}, respectively, which is almost three times higher than those of the PAN-50, PVC-50, and PVDF-50 membranes. Consequently, their electrical resistance values are 3.1 and 3.9 Ω·cm^2, respectively, which are three to four times lower than those observed for the membranes investigated in this study. This can limit the application of the manufactured membranes at high current density since a higher electrical resistance results in a higher energy consumption [53].

4.1.4. Contact angle analysis

The hydrophobic nature of the PAN-50 and PVC-50 membranes was investigated by determining their contact angles, measured through the captive bubble method. In Fig. 2, the obtained values are reported and compared with those of the PVDF-50 membranes described in our previous work [53]. The observed contact angle trend PVDF-50 > PVC-50 > PAN-50 can be attributed to the different nature of the polymers employed, where the use of more hydrophobic polymers imparts a larger hydrophobicity to the membrane.

The contact angle values displayed in Fig. 2 for the three membranes are considerably higher than those of the two commercial AMX and ACS membranes, which were reported to be 26° and 52°, respectively [53]. Generally, by increasing the *IEC*, a membrane becomes more

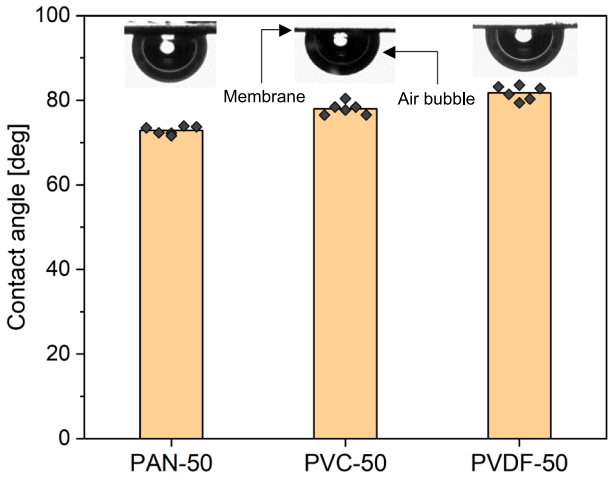

Fig. 2. Contact angle values obtained through captive bubble method for the PAN-50, PVC-50, and PVDF-50 membranes; optical images of the membranes and air bubbles are provided on top of each bar .

hydrophilic due to the increased amount of charged moieties [78,82]. As a result, membranes with higher *IEC* values tend to have typically higher water content [78–82,89], as we also observed in our previous study [25]. As previously discussed, the *IEC* values of the AMX and ACS membranes are higher than those of PAN-50, PVC-50, and PVDF-50. This indicates that a strategy to increase the hydrophobicity of a membrane is decreasing its *IEC*. Along these lines, Tekinalp *et al.* [22] modified poly(2,6-dimethyl-1,4-phenylene oxide) by introducing quaternary ammonium groups using trimethylamine to produce AEMs. Specifically, increasing the functionalization reaction temperature enabled them to increase the incorporation of quaternary ammonium groups into the polymeric backbone, thereby increasing the *IEC*. Their examination of water contact angles and *WU* revealed a reduction in membrane hydrophobicity.

4.1.5. SEM-EDX analysis

The SEM images of the PVDF-50, PVC-50, and PAN-50 membranes, obtained with a magnification of × 1,000, along with their respective EDX analyses, are presented in Fig. 3. Additional SEM images at × 500 and × 1,500 magnifications are provided in **Figure S2** of the Supporting Information. All membranes present a compact structure without visible voids. The EDX analysis focused on the distribution of fluorine (F), chlorine (Cl), and nitrogen (N) respectively in the PVDF-50 (Fig. 3**a1**), PVC-50 (Fig. 3**b1**), and PAN-50 (Fig. 3**c1**) membranes. The images confirm a similar and even distribution of the three polymers within the membranes. The presence of oxygen (O) and bromine (Br) in the EDX analysis can be attributed to the ionomer (Fumion FAS-24), which also turns out to be evenly distributed. The assignment that goes along with this elemental mapping is supported by the analysis of a polymer-free membrane containing this component exclusively, as illustrated in **Figure S3** of the Supporting Information.

4.2. Membrane performance

4.2.1. Permselectivity and permeability coefficient ratio

Fig. 4 displays the measured values of permselectivity and permeability coefficient ratio for the three membranes. Notably, all membranes exhibit a permselectivity value exceeding 90 %, a result that is consistent with existing literature [70].

While the permeability coefficient ratio of the PVDF-50 and PVC-50 membranes are as high as 3 and similar, the one of PAN-50 was found to be lower (Fig. 4). Despite this difference, all membranes possess a higher

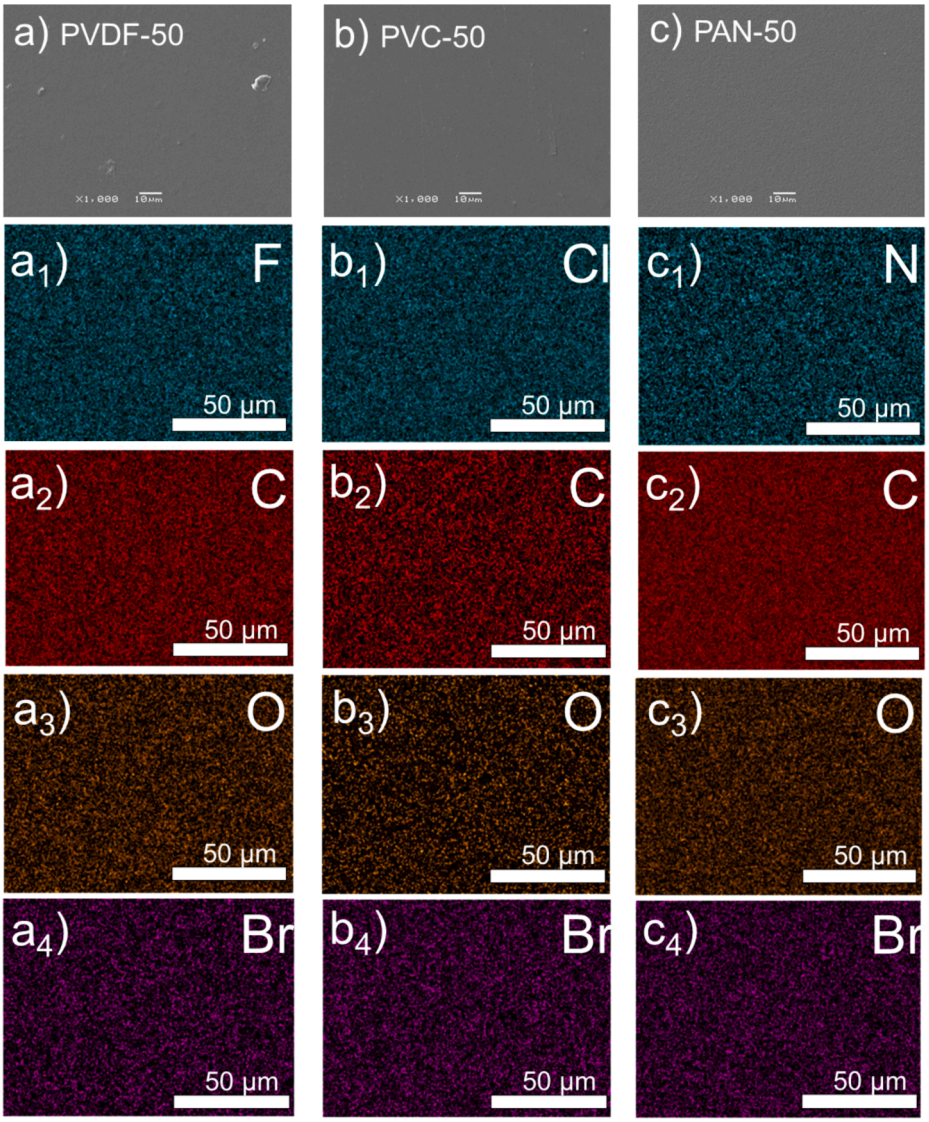

Fig. 3. SEM images obtained with a magnification of × 1,000 for **a)** PVDF-50, **b)** PVC-50, and **c)** PAN-50. Images of the EDX analysis for each membrane are placed below the SEM images. The images with subscript 2, 3, and 4, indicate the element carbon (C), oxygen (O), and bromide (Br) for all membranes, while with subscript 1 we refer to fluorine (F) for the PVDF-50 membrane, to chlorine (Cl) for the PVC-50 membrane , to nitrogen (N) for the PAN-50 membrane.

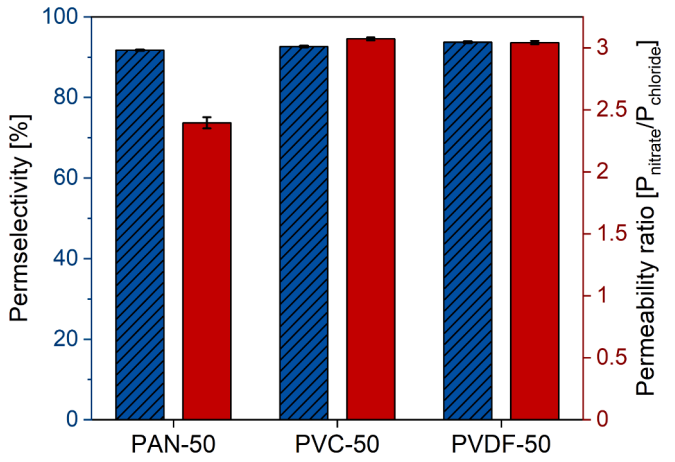

Fig. 4. Permselectivity and permeability coefficient ratio values of the PAN-50, PVC-50, and PVDF-50 membranes. Experiments have been conducted in triplicate.

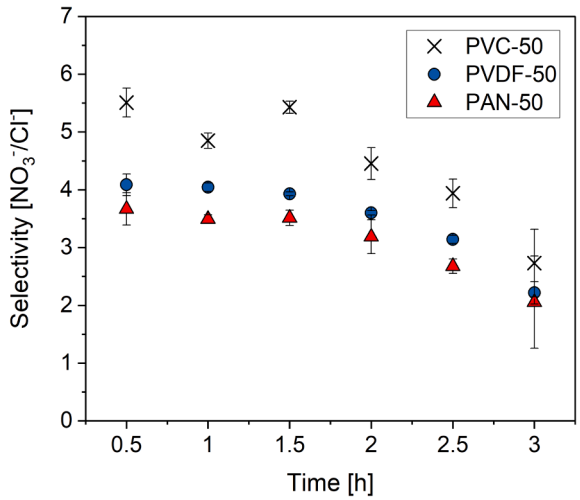

Fig. 5. Trends of the nitrate over chloride selectivity obtained by ED for the PVC-50 and PAN-50 membranes manufactured in this study, along with that of the PVDF-50 membrane reported in our previous work. Experiments were repeated in triplicate for each membrane.

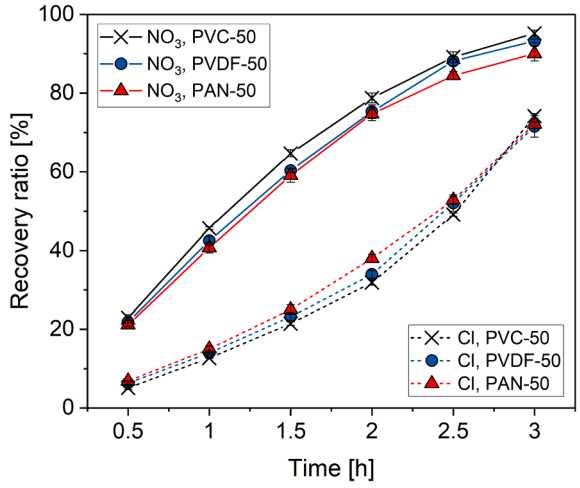

Fig. 6. Trends of the recovery ratio of nitrate (solid lines) and chloride (dashed lines) obtained by ED for the two manufactured PVC-50 and PAN-50 membranes, along with those of the PVDF-50 membrane reported in our previous work.

permeability compared to those of the two commercial membranes AMX and ACS (1.5 and 1.9, respectively [53]). The reduced value for PAN-50 can be attributed to its lower surface hydrophobicity, leading to a decreased affinity between nitrate and the membrane. On the other hand, given the observed differences in hydrophobicity for PVDF-50 and PVC-50, one might have expected a higher value for the former than the latter. Therefore, while this method serves as a quick indicator of a membrane's selective behaviour [74], we proceed conducting electrodialysis experiments for a more precise determination of selectivity.

4.2.2. ED experiments

In this section, we present the experimental results of the transport of nitrate and chloride through the PVC-50 and PAN-50 membranes, obtained in batch-mode electrodialysis. These results are compared with those obtained in our previous work for the membrane PVDF-50 [53]. Over time, we observed changes in the levels of nitrate and chloride in the two reservoirs for the two membranes (refer to Supporting Information **Figure S4**). The concentrations increased in the concentrate reservoir and declined in the diluate reservoir, with the nitrate showing a higher increasing rate than the chloride in the concentrate reservoir. The coulombic efficiency for all experiments was in the range of 93–97 %.

The nitrate over chloride selectivity was calculated over time according to **Eq. (9)**, and the values obtained are presented in Fig. 5 along with those of the PVDF-50 membrane. The data highlights that the PVC-50 membrane exhibits the highest selectivity, while PVDF-50 and PAN-50 show comparable selectivity, albeit with slightly lower values for PAN-50. This is further evident when analyzing the trends of the nitrate and chloride recovery ratios over time, as shown in Fig. 6 and obtained using **Eq. (11)**. Specifically, while the PAN-50 membrane exhibits slightly lower nitrate recovery compared to PVDF-50, the PVC-50 membrane allows for higher nitrate recovery and lower chloride recovery. Moreover, we can also observe that for all membranes, after 2 h, corresponding to a 60 % degree of desalination, the rate of nitrate increase becomes lower, while the rate of chloride increases than in the previous 2 h, as reflected by the changes of the slopes in Fig. 6. This is attributed to the faster nitrate depletion compared to chloride in the diluate, where the remaining nitrate quantity is not sufficient to sustain the fixed ionic flux of 3 mmol·h^{-1}. Indeed, the residual amounts of nitrate and chloride in the diluate at 2 h for the PVC-50 membrane are 1.0 and 3.1 mmol, respectively. Thus, with a flux of 3 mmol·h^{-1}, it is evident that nitrate alone is not sufficient to sustain the flux. Therefore, while extending the ED for a longer duration may indeed lead to higher nitrate recovery, it should be noted that this comes at the cost of increased chloride contamination.

Compared to the selectivity values of the commercial membranes reported in one of our previous studies (selectivity values from ~1.8 to ~1.2 for AMX and ~2.8 to ~1.3, from 0.5 to 3 h, respectively) [53], at any time, the selectivity values of all three membranes are higher (Fig. 5). This supports the efficacy of reducing the *IEC* by incorporating non-charged polymers to increase the membrane's hydrophobicity and thus achieve improved nitrate selectivity.

As mentioned in the introduction, our initial decision to use a polymer with intrinsic hydrophobic characteristics such as PVDF was influenced by its extensive use in membrane technology and by existing literature suggesting a correlation between increased membrane hydrophobicity and enhanced nitrate selectivity. Our previous studies [25,53] confirmed that higher concentrations of PVDF indeed result in increased nitrate selectivity and we associated this effect to the increased membrane's hydrophobicity as reflected by the contact angle obtained compared to those of AMX and ACS. Therefore, based on these findings, we expected the PVDF-50 membrane to outperform PVC-50 and PAN-50, given its higher surface hydrophobicity, as illustrated in Fig. 2. However, the results reported in the current study suggest that

while an increased membrane hydrophobicity is crucial for enhancing nitrate selectivity, other factors should also be evaluated. Specifically, we recommend also considering the membrane's *FCC*. Previous research conducted by Epsztein *et al.* [23] highlighted the role of dehydration-induced adsorption at the water-membrane interface in ion selectivity. However, they also proposed that ions with a lower dehydration energy, such as nitrate, form stronger interactions with the membrane's charged groups, resulting in slower diffusion.

Therefore, by analyzing the fixed charge concentration of the three membranes (Table 2), we hypothesize that despite PVDF's higher surface hydrophobicity favoring nitrate adsorption over chloride, its elevated *FCC* hinders nitrate diffusion due to increased interaction with the membrane's charged groups. On the other hand, while the PAN-50 membrane presents the lowest surface hydrophobicity, its *FCC* is also the lowest observed in the series of investigated polymers, which can explain the similarity in the selectivity data of the PAN-50 and PVDF-50 membranes, though slightly lower. Therefore, we hypothesize that the PVC-50 membrane strikes a balance between surface hydrophobicity and *FCC*, making it – within the window of chosen polymers – the optimal choice for improved nitrate selectivity.

The higher selectivity displayed by the PVC-50 membrane presents an opportunity for further research. Based on our previous studies [52,53], which correlated a higher PVDF concentration with a higher nitrate selectivity, we hypothesize that by using PVC one can achieve selectivity values similar to those of the PVDF-50 membrane but with a lower percentage of polymer used.

Additionally, further membrane development is expected to benefit from obtaining a more detailed current–voltage characteristics, e.g. along the lines of a recent contribution of Zimmerman *et al.* [90] which investigated the role of the limiting current density (*LCD*) as a selectivity promoter in removing target ions from concentrated solutions using ED. In this study, the boundary-layer method was introduced to determine ion-specific *LCD* values and by operating the ED unit at the specific *LCD*s of target ions, the impact on the separation efficiency between counterions was demonstrated. This approach promoted monovalent selectivity in a multi-ionic mixture containing chloride, fluoride, and sulfate while minimizing energy consumption. These insights are valuable in exploring the performance of future membranes and optimizing their selectivity and efficiency across varying current densities.

Lastly, it is worth noting that the energy consumption values calculated using **Eq. (12)** for the three manufactured membranes (PVDF-50, PVC-50, and PAN-50) are about 20–35 % higher than those obtained in our previous study [53] for the two commercial membranes, AMX and ACS (Table 3). However, we consider the increased energy consumption to be a reasonable trade-off given that the three manufactured membranes exhibit higher selectivity than the commercial ones.

Table 3
Energy consumption obtained for the batch-mode ED experiments at 20 $A \cdot m^{-2}$ for the PVDF-50, PVC-50, PAN-50, ACS, and AMX membranes.

	PVDF-50	PVC-50	PAN-50	ACS	AMX
E ($kJ \cdot g^{-1}$ NO_3)	0.57	0.61	0.60	0.48	0.45

5. Conclusion

To identify more environmentally sustainable polymers for AEMs with enhanced nitrate selectivity, we explored PVC and PAN as alternatives to PVDF, which previously demonstrated the best-reported nitrate selectivity. Via a casting process using PVC and PAN in combination with an ionomer solution, two AEMs were manufactured successfully.

Our findings show that all membranes have higher nitrate selectivity than the commercially available ones. This is attributed to increased hydrophobicity, which enhances membrane-nitrate affinity. Among the polymers investigated, the PVC-based membrane outperforms both the PVDF and PAN-based ones, with the latter having slightly lower selectivity than the former.

Considering the superior hydrophobic nature of the PVDF membrane, the correlation "increased hydrophobicity = increased nitrate selectivity" alone does not explain the higher nitrate-selective performance of the PVC membrane. We, therefore, examined the difference in fixed charge concentration between the membranes, suggesting its influence on the selectivity mechanism. Specifically, membranes with higher fixed charge concentrations, like the PVDF one, provide more opportunities for mobile ions to interact with fixed charges. Consequently, the mobility of less hydrated ions like nitrate, is impeded, leading to lower diffusion rates compared to more hydrated ions like chloride.

In conclusion, our study suggests balancing hydrophobicity and fixed charge concentration in membrane manufacturing to achieve optimal nitrate selectivity.

Declaration of competing interest

The authors declare that they have no known competing financial interests or personal relationships that could have appeared to influence the work reported in this paper.

Data availability

Data will be made available on request.

Acknowledgments

The authors thank the Dutch Research Council – Wetsus Partnership Programme on Sustainable Water Technology for funding this project (ALWET.2019.004). This work was performed in the cooperation framework of Wetsus, European Centre of Excellence for Sustainable Water Technology, the Netherlands (www.wetsus.nl). Wetsus is co-funded by the Dutch Ministry of Economic Affairs and Ministry of Infrastructure and Environment, the European Union Regional Development Fund, the Province of Fryslân and the Northern Netherlands Provinces. The authors like to thank the participants of the research theme "Desalination & Concentrates" for the fruitful discussions and their financial support.

Appendix A. Supplementary material

Supplementary material to this article can be found online at https://doi.org/10.1016/j.seppur.2024.129440.

References

[1] D.V. Golubenko, A.D. Manin, Y. Wang, T. Xu, A.B. Yaroslavtsev, The way to increase the monovalent ion selectivity of fujifilm® anion-exchange membranes by cerium phosphate modification for electrodialysis desalination, Desalination 531 (2022) 115719, https://doi.org/10.1016/j.desal.2022.115719.
[2] Z. Qian, H. Miedema, L.C.P.M. de Smet, E.J.R. Sudhölter, Permeation selectivity in the electro-dialysis of mono- and divalent cations using supported liquid membranes, *Desalination* 521 (2022), https://doi.org/10.1016/j.desal.2021.115398.
[3] M. Sedighi, M.M. Behvand Usefi, A.F. Ismail, M. Ghasemi, Environmental sustainability and ions removal through electrodialysis desalination: operating conditions and process parameters, Desalination 549 (2023) 116319, https://doi.org/10.1016/j.desal.2022.116319.
[4] T.M. Khoi, N.A.T. Tran, H.B. Jung, V.P. Huynh, Y. Kim, J. Hong, C.-Y. Yoo, H. S. Kang, Y. Cho, Selective and continuous ion recovery using flow electrode capacitive deionization with polymer multilayers functionalized ion exchange membrane, Desalination 558 (2023) 116626, https://doi.org/10.1016/j.desal.2023.116626.
[5] J.G. Gamaethiralalage, L.C.P.M. de Smet, Rocking-chair capacitive deionization for phosphate recovery *via* rejection mode using ion-exchange membranes, Desalination 564 (2023) 116752, https://doi.org/10.1016/j.desal.2023.116752.
[6] H. Zhang, Y. Li, J. Han, Y. Sun, M. He, Z. Hao, T. Jiang, B. Wang, W. Wang, M. Liu, Influence of ion exchange membrane arrangement on dual-channel flow electrode

capacitive deionization: theoretical analysis and experimentations, Desalination 548 (2023) 116288, https://doi.org/10.1016/j.desal.2022.116288.
[7] Z. Yu, W.-C. Tsen, T. Qu, F. Cheng, F. Hu, H. Liu, S. Wen, C. Gong, Highly ion-conductive anion exchange membranes with superior mechanical properties based on polymeric ionic liquid filled functionalized bacterial cellulose for alkaline fuel cells, J. Mater. Res. Technol. 23 (2023) 6187–6199, https://doi.org/10.1016/j.jmrt.2023.02.197.
[8] D. Li, W. Chu, J. Wei, Y. Hu, Y. He, H. Qin, J. Liu, J. He, H. Ni, Effects of hydrolysis degree on ion-doped anion exchange membranes in direct borohydride fuel cells, Int. J. Hydrogen Energy 48 (69) (2023) 26990–27000, https://doi.org/10.1016/j.ijhydene.2023.03.235.
[9] A. Campione, L. Gurreri, M. Ciofalo, G. Micale, A. Tamburini, A. Cipollina, Electrodialysis for water desalination: a critical assessment of recent developments on process fundamentals models and applications, *Desalination* 2018 (434) (2017) 121–160, https://doi.org/10.1016/j.desal.2017.12.044.
[10] A.-A. Sajjad, M.Y.B.M. Yunus, A.A.M. Azoddein, D.G. Hassell, I.H. Dakhil, H. A. Hasan, Electrodialysis desalination for water and wastewater: a review, Chem. Eng. J. 2019 (380) (2019) 122231, https://doi.org/10.1016/j.cej.2019.122231.
[11] S. Al-Amshawee, M.Y.B.M. Yunus, A.A.M. Azoddein, D.G. Hassell, I.H. Dakhil, H. A. Hasan, Electrodialysis desalination for water and wastewater: a review, Chem. Eng. J. 380 (2020) 122231, https://doi.org/10.1016/j.cej.2019.122231.
[12] T. Luo, S. Abdu, M. Wessling, Selectivity of ion exchange membranes: a review, J. Membrane Sci. 2018 (555) (2017) 429–454, https://doi.org/10.1016/j.memsci.2018.03.051.
[13] D. Chinello, A. Myrstad, L.C.P.M. de Smet, H. Miedema, Modelling the required membrane selectivity for NO^{3-} recovery from effluent also containing Cl^{-}, while saving water, Chem. Eng. Res. Design 193 (2023) 409–419, https://doi.org/10.1016/j.cherd.2023.03.038.
[14] Z. Qian, H. Miedema, L.C.P.M. de Smet, E.J.R. Sudhölter, Modelling the selective removal of sodium ions from greenhouse irrigation water using membrane technology, Chem. Eng. Res. Des. 134 (2018) 154–161, https://doi.org/10.1016/j.cherd.2018.03.040.
[15] T. Mubita, S. Porada, P. Aerts, A. van der Wal, Heterogeneous anion exchange membranes with nitrate selectivity and low electrical resistance, J. Membr. Sci. 607 (2020) 118000, https://doi.org/10.1016/j.memsci.2020.118000.
[16] T.M. Mubita, S. Porada, P.M. Biesheuvel, A. van der Wal, J.E. Dykstra, Strategies to increase ion selectivity in electrodialysis, Sep. Purif. Technol. 292 (2022) 120944, https://doi.org/10.1016/j.seppur.2022.120944.
[17] T. Kikhavani, S.N. Ashrafizadeh, B. Van Der Bruggen, Nitrate selectivity and transport properties of a novel anion exchange membrane in electrodialysis, Electrochim. Acta 144 (2014) 341–351, https://doi.org/10.1016/j.electacta.2014.08.012.
[18] C.-M. Oh, C.-W. Hwang, T.-S. Hwang, Synthesis of a quaternarized poly (vinylimidazole-co-trifluoroethylmethacrylate-co-divinylbenzene) anion-exchange membrane for nitrate removal, J. Environ. Chem. Eng. 2 (4) (2014) 2162–2169, https://doi.org/10.1016/j.jece.2014.09.014.
[19] N. Zhang, H. Yu, J. Zhang, X. Jiang, S. Yin, G. Zhou, X. Zhang, J. Bao, G. He, Pressure-driven Li^{+}/Mg^{2+} selective permeation through size-sieving nanochannels: the role of the second hydration shell, Sep. Purif. Technol. 327 (2023) 124818, https://doi.org/10.1016/j.seppur.2023.124818.
[20] M. Irfan, L. Ge, Y. Wang, Z. Yang, T. Xu, Hydrophobic side chains impart anion exchange membranes with high monovalent-divalent anion selectivity in electrodialysis, ACS Sustain. Chem. Eng. 7 (4) (2019) 4429–4442, https://doi.org/10.1021/acssuschemeng.8b06426.
[21] T. Sata, Studies on anion exchange membranes having permselectivity for specific anions in electrodialysis - effect of hydrophilicity of anion exchange membranes on permselectivity of anions, J. Membr. Sci. 167 (1) (2000) 1–31, https://doi.org/10.1016/S0376-7388(99)00277-X.
[22] Ö. Tekinalp, P. Zimmermann, O.S. Burheim, L. Deng, Designing monovalent selective anion exchange membranes for the simultaneous separation of chloride and fluoride from sulfate in an equimolar ternary mixture, J. Membr. Sci. 666 (2023) 121148, https://doi.org/10.1016/j.memsci.2022.121148.
[23] R. Epsztein, E. Shaulsky, M. Qin, M. Elimelech, Activation behavior for ion permeation in ion-exchange membranes: role of ion dehydration in selective transport, J. Membr. Sci. 580 (2019) 316–326, https://doi.org/10.1016/j.memsci.2019.02.009.
[24] R. Epsztein, R.M. DuChanois, C.L. Ritt, A. Noy, M. Elimelech, Towards single-species selectivity of membranes with subnanometre pores, Nat. Nanotechnol. 15 (6) (2020) 426–436, https://doi.org/10.1038/s41565-020-0713-6.
[25] D. Chinello, J. Post, L.C.P.M. de Smet, Selective separation of nitrate from chloride using PVDF-based anion-exchange membranes, Desalination 572 (2024) 117084, https://doi.org/10.1016/j.desal.2023.117084.
[26] D. Zou, L. Xia, P. Luo, K. Guan, H. Matsuyama, Z. Zhong, Fabrication of hydrophobic Bi-layer fiber-aligned PVDF/PVDF-PSF membranes using green solvent for membrane distillation, Desalination 565 (2023) 116810, https://doi.org/10.1016/j.desal.2023.116810.
[27] G.H. Teoh, Z.A. Jawad, D.J.C. Chan, S.C. Low, Surface regeneration of templated PVDF membrane for efficient microalgae-rich high saline aquaculture wastewater treatment in membrane distillation, Desalination 565 (2023) 116858, https://doi.org/10.1016/j.desal.2023.116858.
[28] H.-R. Yang, Y.-H. Huang, C.-F. Wang, T.-S. Chung, Green fabrication of PVDF superhydrophobic membranes using a green solvent triethyl phosphate (TEP) for membrane distillation, Desalination 566 (2023) 116934, https://doi.org/10.1016/j.desal.2023.116934.
[29] W. Jankowski, W. Kujawski, J. Kujawa, Spicing up membrane distillation: enhancing PVDF membrane performance with cinnamic acid, Desalination 575 (2024) 117304, https://doi.org/10.1016/j.desal.2024.117304.
[30] J. Xu, K. Guan, P. Luo, S. He, H. Matsuyama, D. Zou, Z. Zhong, Engineering PVDF omniphobic membranes with flower-like micro-nano structures for robust membrane distillation, Desalination 578 (2024) 117442, https://doi.org/10.1016/j.desal.2024.117442.
[31] M. Namdari, F. Zokaee Ashtiani, E. Bonyadi, Development of a high flux janus PVDF membrane for oily saline water desalination by membrane distillation via PDA-TEOS-APTES surface modification, Desalination 572 (2024) 117139, https://doi.org/10.1016/j.desal.2023.117139.
[32] B. Sun, M. Wu, H. Zhen, Y. Jia, P. Li, Z. Yuan, X. Li, G. He, X. Jiang, Tailored PVDF membrane with coordinated interfacial nano/micro-structure for enhanced membrane distillation, Desalination 573 (2024) 117177, https://doi.org/10.1016/j.desal.2023.117177.
[33] Q. Luo, L. Huang, P. Yun, T. Qiu, B. Tang, K. Huang, X. Hu, H. Jiang, Thermal-driven osmosis utilizing hollow fiber membranes: sustainable dye water treatment and electricity extraction, Desalination 579 (2024) 117485, https://doi.org/10.1016/j.desal.2024.117485.
[34] P. Zhang, S. Rajabzadeh, Q. Song, R.R. Gonzales, Y. Jia, S. Xiang, Z. Li, H. Matsuyama, Development of loose nanofiltration PVDF hollow fiber membrane for dye/salt separation, Desalination 549 (2023) 116315, https://doi.org/10.1016/j.desal.2022.116315.
[35] C. Wang, Y. Chen, X. Hu, X. Feng, In-situ synthesis of PA/PVDF composite hollow fiber membranes with an outer selective structure for efficient fractionation of low-molecular-weight dyes-salts, Desalination 503 (2021) 114957, https://doi.org/10.1016/j.desal.2021.114957.
[36] Y. Zhao, J. Guo, Y. Li, X. Zhang, A.K. An, Z. Wang, Superhydrophobic and superoleophilic PH-CNT membrane for emulsified oil-water separation, Desalination 526 (2022) 115536, https://doi.org/10.1016/j.desal.2021.115536.
[37] J. Gao, M. Cai, Z. Nie, J. Zhang, Y. Chen, Superwetting PVDF membrane prepared by in situ extraction of metal ions for highly efficient oil/water mixture and emulsion separation, Sep. Purif. Technol. 275 (2021) 119174, https://doi.org/10.1016/j.seppur.2021.119174.
[38] K.H. Lee, I.A. Khan, L.H. Song, J.Y. Kim, J.-O. Kim, Evaluation of structural/performance variation between α-Al_2O_3 and polyvinylidene fluoride membranes under long-term clean-in-place treatment used for water treatment, Desalination 538 (2022) 115921, https://doi.org/10.1016/j.desal.2022.115921.
[39] A. Asadi, F. Gholami, S. Nazari, M. Dolatshah, Improved filtration performance of polyvinylidene fluoride nanocomposite membranes embedded with deep eutectic solvent: application towards MBR, Desalination 543 (2022) 116088, https://doi.org/10.1016/j.desal.2022.116088.
[40] M.S. Khan, Y. Li, L. Yang, Z.C. Yan, D.-S. Li, J. Qiu, X. Xu, H.Y. Yang, Improving capacitive deionization performance through tailored iodine-loaded ZIF-8 composites, Desalination (2024) 117486, https://doi.org/10.1016/j.desal.2024.117486.
[41] T.M. Khoi, J. Kim, N.A.T. Tran, V.P. Huynh, Y.-W. Lee, Y. Cho, Redox flow deionization using prussian blue and functionalized ion exchange membrane for enhanced selective ion recovery, Desalination 578 (2024) 117444, https://doi.org/10.1016/j.desal.2024.117444.
[42] L. Zhang, T. Zhang, S. Lv, S. Song, H.J.O. Galván, M. Quintana, Y. Zhao, Adsorbents for lithium extraction from salt lake brine with high magnesium/lithium ratio: from structure-performance relationship to industrial applications, Desalination 579 (2024) 117480, https://doi.org/10.1016/j.desal.2024.117480.
[43] K. Sharma, N. Akther, Y. Choo, P. Zhang, H. Matsuyama, H.K. Shon, G. Naidu, Positively charged nanofiltration membranes for enhancing magnesium separation from seawater, Desalination 568 (2023) 117026, https://doi.org/10.1016/j.desal.2023.117026.
[44] J. Jiang, P. Dorji, U. Badeti, W. Sohn, S. Freguia, S. Phuntsho, I. El Saliby, H. K. Shon, Potential nutrient recovery from source-separated urine through hybrid membrane bioreactor and membrane capacitive deionisation, Desalination 566 (2023) 116924, https://doi.org/10.1016/j.desal.2023.116924.
[45] N. Han, Y. Li, H. Peng, R. Gao, Q. He, Z. Miao, K. Wan, Adsorption of Li+ by imprinted capacitor deionization — a new method for selective recovery of valuable lithium in acidic solutions, Desalination 565 (2023) 116820, https://doi.org/10.1016/j.desal.2023.116820.
[46] W. Wang, P. Ma, H. Li, Cationic segregation of $Ca_2Mn_3O_8$ enabling high selectivity for fluoride ions through capacitive deionization, Desalination 564 (2023) 116798, https://doi.org/10.1016/j.desal.2023.116798.
[47] H.M.T.R. Shirazi, A. Heidari, T. Mohammadi, Fabrication of high-performance mei and HPEI assembled PES/CPES hollow fiber nanofiltration membranes with high positive charges for efficient removal of salt/heavy metal ions, Desalination 565 (2023) 116877, https://doi.org/10.1016/j.desal.2023.116877.
[48] S. Mishra, A.K. Singh, J.K. Singh, Ferrous sulfide and carboxyl-functionalized ferroferric oxide incorporated PVDF-based nanocomposite membranes for simultaneous removal of highly toxic heavy-metal ions from industrial ground water, J. Membr. Sci. 593 (2020) 117422, https://doi.org/10.1016/j.memsci.2019.117422.
[49] C. Simari, E. Lufrano, G. Lemes, M.J. Lázaro, D. Sebastián, I. Nicotera, Electrochemical performance and alkaline stability of cross-linked quaternized polyepichlorohydrin/PvDF blends for anion-exchange membrane fuel cells, J. Phys. Chem. C 125 (10) (2021) 5494–5504, https://doi.org/10.1021/acs.jpcc.0c11346.
[50] P.P. Sharma, V. Yadav, A. Rajput, V. Kulshrestha, PVDF-g-Poly (styrene-co-vinylbenzyl chloride) based anion exchange membrane: high salt removal

efficiency and stability, Desalination 444 (2018) 35–43, https://doi.org/10.1016/j.desal.2018.07.002.
[51] P.P. Sharma, V. Yadav, A. Rajput, V. Kulshrestha, Acid resistant PVDF based copolymer alkaline anion exchange membrane for acid recovery and electrodialytic water desalination, J. Membr. Sci. 563 (2018) 561–570, https://doi.org/10.1016/j.memsci.2018.06.016.
[52] D. Chinello, J. Post, L.C.P.M. de Smet, Selective separation of nitrate from chloride using PVDF-based anion-exchange membranes, Desalination (2023) 117084, https://doi.org/10.1016/j.desal.2023.117084.
[53] D. Chinello, L.C.P.M. de Smet, J. Post, Selective electrodialysis: targeting nitrate over chloride using PVDF-based AEMs, Sep. Purif. Technol. 342 (2024) 126885, https://doi.org/10.1016/j.seppur.2024.126885.
[54] M.N. Ehsan, M. Riza, M.N. Pervez, C.-W. Li, A.A. Zorpas, V. Naddeo, PFAS contamination in soil and sediment: contribution of sources and environmental impacts on soil biota, Case Stud. Chem. Environ. Eng. 9 (2024) 100643, https://doi.org/10.1016/j.cscee.2024.100643.
[55] P.A. Novak, S.D. Hoeksema, S.N. Thompson, K.M. Trayler, Per- and Polyfluoroalkyl Substances (PFAS) contamination in a microtidal urban estuary: sources and sinks, Mar. Pollut. Bull. 193 (2023) 115215, https://doi.org/10.1016/j.marpolbul.2023.115215.
[56] M. Sadia, M. Kunz, T. ter Laak, M. De Jonge, M. Schriks, A.P. van Wezel, Forever legacies? Profiling Historical PFAS contamination and current influence on groundwater used for drinking water, Sci. Total Environ. 890 (2023) 164420, https://doi.org/10.1016/j.scitotenv.2023.164420.
[57] K. Singh, N. Kumar, A. Kumar Yadav, R. Singh, K. Kumar, Per-and Polyfluoroalkyl Substances (PFAS) as a health hazard: current state of knowledge and strategies in environmental settings across asia and future perspectives, Chem. Eng. J. 475 (2023) 145064, https://doi.org/10.1016/j.cej.2023.145064.
[58] K.L. Smalling, K.M. Romanok, P.M. Bradley, M.C. Morriss, J.L. Gray, L.K. Kanagy, S.E. Gordon, B.M. Williams, S.E. Breitmeyer, D.K. Jones, L.A. DeCicco, C.A. Eagles-Smith, T. Wagner, Per- and polyfluoroalkyl substances (PFAS) in United States Tapwater: Comparison of underserved private-well and public-supply exposures and associated health implications, Environ. Int. 178 (2023) 108033, https://doi.org/10.1016/j.envint.2023.108033.
[59] J. Maiti, N. Kakati, P. Basumatary, S.P. Woo, Y.S. Yoon, Imidazolium Functionalized Poly(Vinyl Chloride-Co-Vinyl Acetate)-based anion exchange membrane, Int. J. Hydrogen Energy 41 (13) (2016) 5776–5782, https://doi.org/10.1016/j.ijhydene.2016.02.062.
[60] K. Khoiruddin, D. Ariono, S. Subagjo, I.g. Wenten, Structure and transport properties of polyvinyl chloride-based heterogeneous cation-exchange membrane modified by additive blending and sulfonation, J. Electroanal. Chem. 873 (2020) 114304, https://doi.org/10.1016/j.jelechem.2020.114304.
[61] T. Ahmad, C. Guria, Progress in the modification of polyvinyl chloride (PVC) membranes: a performance review for wastewater treatment, J. Water Process Eng. 45 (2022) 102466, https://doi.org/10.1016/j.jwpe.2021.102466.
[62] M. Safarpour, A. Safikhani, V. Vatanpour, Polyvinyl chloride-based membranes: a review on fabrication techniques, applications and future perspectives, Sep. Purif. Technol. 279 (2021) 119678, https://doi.org/10.1016/j.seppur.2021.119678.
[63] M. Nemati, S.M. Hosseini, E. Bagheripour, S.S. Madaeni, Electrodialysis heterogeneous anion exchange membranes filled with TiO_2 nanoparticles: membranes' fabrication and characterization, J. Membrane Sci. Res. 1 (3) (2015) 135–140.
[64] Y. Liu, J. Liao, G. Peng, C. Dong, S. Yang, J. Shen, Poly(Vinyl Chloride)-based anion-exchange membrane with high-antifouling potential for electrodialysis application, ACS Appl. Polym. Mater. 3 (5) (2021) 2529–2540, https://doi.org/10.1021/acsapm.1c00121.
[65] M. Zafari, T. Kikhavani, S.N. Ashrafizadeh, Hybrid surface modification of an anion exchange membrane for selective separation of monovalent anions in the electrodialysis process, J. Environ. Chem. Eng. 10 (1) (2022) 107014, https://doi.org/10.1016/j.jece.2021.107014.
[66] A.A. Kishore Chand, B. Bajer, E.S. Schneider, T. Mantel, M. Ernst, V. Filiz, S. Glass, Modification of polyacrylonitrile ultrafiltration membranes to enhance the adsorption of cations and anions, Membranes (Basel) 12 (6) (2022) 580, https://doi.org/10.3390/membranes12060580.
[67] L. Wang, G. Xu, J. Xiao, M. Tao, W. Zhang, Quaternary ammonium-based functionalized polyacrylonitrile fibers with polarity tunable inner surface microenvironment for C-C Bond forming reactions under continuous flow conditions, Ind. Eng. Chem. Res. 58 (27) (2019) 12401–12410, https://doi.org/10.1021/acs.iecr.9b01375.
[68] H. Geng, C. Zhang, M. Tao, N. Ma, W. Zhang, Ionic microenvironment constructed in quaternary ammonium modified polyacrylonitrile fiber for efficient CO_2 fixation, *J. CO_2 Util.* 49 (2021) 101559, https://doi.org/10.1016/j.jcou.2021.101559.
[69] E.R. Nightingale, Phenomenological Theory of Ion Solvation. Effective Radii of Hydrated Ions, *J. Phys. Chem.* 63 (9) (1959) 1381–1387, https://doi.org/10.1021/j150579a011.
[70] P. Dlugolecki, K. Nymeijer, S. Metz, M. Wessling, Current status of ion exchange membranes for power generation from salinity gradients, J. Membr. Sci. 319 (1–2) (2008) 214–222, https://doi.org/10.1016/j.memsci.2008.03.037.
[71] D. Kitto, J. Kamcev, The need for ion-exchange membranes with high charge densities, J. Membr. Sci. 677 (2023) 121608, https://doi.org/10.1016/j.memsci.2023.121608.
[72] A.H. Galama, N.A. Hoog, D.R. Yntema, Method for determining ion exchange membrane resistance for electrodialysis systems, Desalination 380 (2016) 1–11, https://doi.org/10.1016/j.desal.2015.11.018.
[73] Z. Qian, H. Miedema, S. Sahin, L.C.P.M. de Smet, E.J.R. Sudhölter, Separation of Alkali Metal Cations by a Supported Liquid Membrane (SLM) Operating under Electro Dialysis (ED) Conditions, *Desalination* 495 (2020), https://doi.org/10.1016/j.desal.2020.114631.
[74] T. Luo, F. Roghmans, M. Wessling, Ion Mobility and partition determine the counter-ion selectivity of ion exchange membranes, J. Membr. Sci. 597 (2020) 117645, https://doi.org/10.1016/j.memsci.2019.117645.
[75] V.V. Nikonenko, N.D. Pismenskaya, E.I. Belova, P. Sistat, P. Huguet, G. Pourcelly, C. Larchet, Intensive current transfer in membrane systems: modelling, mechanisms and application in electrodialysis, Adv. Colloid Interf. Sci. 160 (1) (2010) 101–123, https://doi.org/10.1016/j.cis.2010.08.001.
[76] P.M. Biesheuvel, S. Porada, M. Elimelech, J.E. Dykstra, Tutorial review of reverse osmosis and electrodialysis, J. Membr. Sci. 647 (2022) 120221, https://doi.org/10.1016/j.memsci.2021.120221.
[77] Q.-B. Chen, Z.-Y. Ji, J. Liu, Y.-Y. Zhao, S.-Z. Wang, J.-S. Yuan, Development of recovering lithium from brines by selective-electrodialysis: effect of coexisting cations on the migration of lithium, J. Membr. Sci. 548 (2018) 408–420, https://doi.org/10.1016/j.memsci.2017.11.040.
[78] A.S. Gangrade, S. Cassegrain, P. Chandra Ghosh, S. Holdcroft, Permselectivity of ionene-based, aemion® anion exchange membranes, J. Membr. Sci. 641 (2022) 119917, https://doi.org/10.1016/j.memsci.2021.119917.
[79] A.C.C. Yang, R. Narimani, Z. Zhang, B.J. Frisken, S. Holdcroft, Controlling crystallinity in graft ionomers, and its effect on morphology, water sorption, and proton conductivity of graft ionomer membranes, Chem. Mater. 25 (9) (2013) 1935–1946, https://doi.org/10.1021/cm4005932.
[80] F.G. Wilhelm, I.G.M. Pünt, N.F.A. van der Vegt, H. Strathmann, M. Wessling, Cation permeable membranes from blends of sulfonated poly(ether ether ketone) and poly(ether sulfone), J. Membr. Sci. 199 (1) (2002) 167–176, https://doi.org/10.1016/S0376-7388(01)00695-0.
[81] W. Li, F. Yang, Z. Lin, R. Sun, L. Chen, Y. Xie, J. Pang, Z. Jiang, Semi-crystalline sulfonated poly(ether ketone) proton exchange membranes: the trade-off of facile synthesis and performance, J. Colloid Interf. Sci. 645 (2023) 493–501, https://doi.org/10.1016/j.jcis.2023.04.116.
[82] J. Kamcev, D.R. Paul, B.D. Freeman, Effect of fixed charge group concentration on equilibrium ion sorption in ion exchange membranes, J. Mater. Chem. A 5 (9) (2017) 4638–4650, https://doi.org/10.1039/C6TA07954G.
[83] S. Liang, Y. Kang, A. Tiraferri, E.P. Giannelis, X. Huang, M. Elimelech, Highly hydrophilic polyvinylidene fluoride (PVDF) ultrafiltration membranes via postfabrication grafting of surface-tailored silica nanoparticles, ACS Appl. Mater. Interf. 5 (14) (2013) 6694–6703, https://doi.org/10.1021/am401462e.
[84] G. Kang, Y. Cao, Application and Modification of Poly(Vinylidene Fluoride) (PVDF) Membranes – A Review, J. Membr. Sci. 463 (2014) 145–165, https://doi.org/10.1016/j.memsci.2014.03.055.
[85] Q. Wu, A. Tiraferri, T. Li, W. Xie, H. Chang, Y. Bai, B. Liu, Superwettable PVDF/PVDF-g-PEGMA ultrafiltration membranes, ACS Omega 5 (36) (2020) 23450–23459, https://doi.org/10.1021/acsomega.0c03429.
[86] F.A. Sheikh, M.A. Zargar, A.H. Tamboli, H. Kim, A super hydrophilic modification of poly(Vinylidene Fluoride) (PVDF) nanofibers: by in situ hydrothermal approach, Appl. Surf. Sci. 385 (2016) 417–425, https://doi.org/10.1016/j.apsusc.2016.05.111.
[87] Kaufman, A. A.; Anderson, B. I. Chapter One - Coulomb's Law and Stationary Electric Field. In *Methods in Geochemistry and Geophysics*; Kaufman, A. A., Anderson, B. I., Eds.; Principles of Electric Methods in Surface and Borehole Geophysics; Elsevier, 2010; Vol. 44, pp 3–78. 10.1016/S0076-6895(10)44001-9.
[88] Giorno, L.; Drioli, E.; Strathmann, H. Ion-Exchange Membrane Characterization. In *Encyclopedia of Membranes*; Drioli, E., Giorno, L., Eds.; Springer: Berlin, Heidelberg, 2016; pp 1052–1056. 10.1007/978-3-662-44324-8_994.
[89] J. Kamcev, C.M. Doherty, K.P. Lopez, A.J. Hill, D.R. Paul, B.D. Freeman, Effect of fixed charge group concentration on salt permeability and diffusion coefficients in ion exchange membranes, J. Membr. Sci. 566 (2018) 307–316, https://doi.org/10.1016/j.memsci.2018.08.053.
[90] P. Zimmermann, Ö. Tekinalp, S.B.B. Solberg, Ø. Wilhelmsen, L. Deng, O. S. Burheim, Limiting current density as a selectivity factor in electrodialysis of multi-ionic mixtures, Desalination 558 (2023) 116613, https://doi.org/10.1016/j.desal.2023.116613.